Charging Effects in a CdSe Nanotetrapod

Lin-Wang Wang†

Computational Research Division, Lawrence Berkeley National Laboratory, Berkeley, California 94720

Received: August 4, 2005; In Final Form: September 16, 2005

The charging effects in a CdSe nanotetrapod have been theoretically investigated by using an atomistic pseudopotential method. We showed that the simple quasiparticle equation based on classical electrostatic consideration can be derived from the many-body GW equation under proper approximations. We found that the surface polarization potential can significantly change the electron wave functions, and there is an incomplete cancellation for this potential between the single particle energies and the electron−hole Coulomb interaction. Thus, it is necessary to include this potential in the calculation for complex unconvex systems. We also calculated the electron addition energies for a tetrapod. Unlike a simple spherical quantum dot, in which the addition energies are almost a constant, there is a large variation in the calculated addition energies for different numbers of electrons in a tetrapod.

Charging effects play an important role in electronic device applications of nanosystems. Besides Coulomb blockade and the related tunneling phenomena[1] that affect electron transport, it also affects the optical band gap via the electron−hole interaction. There have been many theoretical studies of the charging effects in nanosystems, e.g., to calculate the addition energies[2] of spherical quantum dots and the electron−hole Coulomb interactions.[3] The employed methods range from effective mass type calculations[4] to atomistic pseudopotential calculations.[2,3] The Coulomb interactions between electrons can be calculated perturbatively after the electron wave functions have been obtained,[2,3] or self-consistently with density functional type methods.[5] Most of the previous studies are focused on simple geometry nanosystems, either spherical quantum dots[2] or tetrahedral quantum dots.[4] There are some distinct consequences of this simple convex geometry. For example, the addition energy is mostly constant after one or two electrons; the surface polarization energy cancels out between the single particle energies and the electron−hole Coulomb interaction.[4] It is interesting to find out whether these are still true for more complicated nanostructures, e.g., the tetrapod.

In recent years, complicated branched nanosystems have been synthesized under wet chemistry.[6,7] One simple example of these branched systems is a tetrapod, consisting of a zinc blende nanocrystal at the center of the structure and four wurtzite crystal arms attached to the four (111) facets of the zinc blende center. Since the system grows coherently in its crystal structure, without a barrier between the zinc blende center and the wurtzite arms, the electron wave function typically extends across these different regions. CdSe and CdTe tetrapods have found their applications in solar cells,[8,9] where the arm structures help to conduct the photoinduced carriers. Recently, conductivity and Coulomb blockade effects have also been measured for the relatively large CdTe tetrapod, with two arms connected to two electrodes.[10] It was found that, depending on the situation, a tetrapod can behave like a single coherent dot or weakly coupled multiple dots. It is interesting to study the charging effect of the tetrapod, and to compare the results to spherical quantum dots. Geometrically, the tetrapod is not convex, which may significantly affect the result of the Poisson equation, thus causing differences in its charging effects. Some of the approximations, e.g., a near constant polarization potential inside a spherical quantum dot,[11] might no longer be correct.

In this work, we will calculate the charging effects of a CdSe nanotetrapod using the atomistic semiempirical pseudopotential method. Compared to previous theoretical works on this topic, the current work has the following differences: (1) the quasiparticle equation originally based on classical electrostatic arguement is derived from the many-body GW equation; (2) a tetrapod geometry nanostructure (which is unconvex) is calculated instead of a simple convex (e.g., spherical) geometry as in most of the previous studies, and the consequence of the unconvexness is discussed; (3) the surface polarization potential is calculated numerically, instead of analytically (which is only possible for simple systems); (4) one fast numerical method to solve the Poisson equation is presented; (5) a configuration interaction method is used to calculate the addition energy, in contrast to a single Slater derminant as used in many previous studies, and (6) the calculated Coulomb blochade results are compared with recent experiment. As in the experiment, we find large fluctuations of the addition energy.

In a previous study,[12] we have calculated the tetrapod electron and hole wave functions under the semiempirical pseudopotential method (SEPM).[13] It was found that the electrons and holes have very different wave functions and they can be located at different places. Here we will use the same SEPM Hamiltonian to study the electron charging effects for the same system. First, the single particle SEPM Hamiltonian for a nanocrystal can be written as

$$\left\{-\frac{1}{2}\nabla^2 + V\right\}\psi_i(r) = E_i\psi_i(r) \qquad (1)$$

Here potential $V = V_{\mathrm{loc}}(r) + \hat{V}_{\mathrm{nonloc}}$ has a local part and a nonlocal part. The local part $V_{\mathrm{loc}}(r) = \sum_{n,\alpha} \upsilon_\alpha(|r - R_{n,\alpha}|)$ is a direct sum of the screened spherical atomic potentials υ_α of atom type α at $R_{n,\alpha}$. The nonlocal part V_{nonloc} includes the s, p, d nonlocal potentials and spin−orbit coupling.[13] Inside the nanocrystal, V is bulklike, while $V = 0$ outside the nanosystem. The electron wave function $\psi_i(r)$ is a spinor with spin up and spin

† E-mail: lwwang@lbl.gov.

10.1021/jp054349q CCC: $30.25
Published on Web 11/19/2005

down components, with each component expanded in a plane-wave basis with a 6.8 Ry kinetic energy cutoff.

Equation 1 is often used as the single particle Schrodinger's equation to solve the electron wave functions of a quantum dot. However, as pointed out by Brus,[11] there is a surface polarization potential $P(r)$ in the true quasiparticle equation. In other words, the quasiparticle equation is

$$\left\{-\frac{1}{2}\nabla^2 + V \pm P(r)\right\}\psi_i(r) = \epsilon_i\psi_i(r) \tag{2}$$

where $+$ is for electron states, and $-$ is for hole states. The quasiparticle energy ϵ_i is defined as $E_{tot}(N+1) - E_{tot}(N)$ for electron and $E_{tot}(N) - E_{tot}(N-1)$ for hole, $E_{tot}(M)$ is the total energy of the nanosystem with M electrons, and $E_{tot}(N)$ is the charge neutral system. On the basis of a classical electrostatic argument, Brus defined $P(r)$ as

$$P(r) = \frac{1}{2}\lim_{r'\to r}[W(r',r) - W_{bulk}(r',r)] \tag{3}$$

where $W(r',r)$ is the screened electrostatic potential of the nanosystem at r' given an external point charge at r, while $W_{bulk}(r',r)$ is the same quantity if the whole space is a bulk, as at the r point. Although eq 2 was originally derived from classical electrostatic arguments, as will be shown below, it can also be derived from the many-body quasiparticle GW equation under proper approximations. A quasiparticle GW equation can be written as[14]

$$\left[-\frac{1}{2}\nabla^2 + \sum_{n,\alpha} v_\alpha^{bare}(|r - R_{n,\alpha}|) + \int \frac{\rho(r')}{|r-r'|}\,d^3r'\right]\psi_i(r) + \int \Sigma(r,r',\epsilon_i)\psi_i(r')\,d^3r' = \epsilon_i\psi_i(r) \tag{4}$$

here the selfenergy Σ is

$$\Sigma(r,r',\omega) = -\sum_j \psi_j(r)\psi_j^*(r')\left[f_j W(r,r',\epsilon_j - \omega) + \frac{1}{\pi}\int_0^\infty \frac{\mathrm{Im}W(r,r',\omega')}{\omega - \epsilon_j - \omega' + i\delta}\,d\omega'\right] \tag{5}$$

f_j is the Fermi−Dirac occupation for state ψ_j and the screened Coulomb potential W, same as in eq 3 (but with a ω dependence), can be written as

$$W(r,r',\omega) = \int \epsilon^{-1}(r,r_1,\omega)\frac{1}{|r_1 - r'|}\,d^3r_1 \tag{6}$$

For a nanocrystal, if r and r' are both inside the nanostructure (where it concerns us most), we can break down $W(r,r',\omega)$ into two parts

$$W(r,r',\omega) = W_{bulk}(r,r',\omega) + P_M(r,r',\omega) \tag{7}$$

The first term W_{bulk} is the bulk screened Coulomb potential and the second term P_M is an additional polarization potential caused by the surface of the nanocrystal. Now if we substitute eq 7 into eq 4, we have

$$H_b^{GW}\psi_i + \int \Sigma_P(r,r',\epsilon_i)\psi_i(r')\,d^3r' = \epsilon_i\psi_i(r) \tag{8}$$

Here H_b^{GW} (caused by substituting W_{bulk} in eqs 5 and 4 inside the nanostructure) is a bulk-like GW Hamiltonian inside the nanostructure, and a free electron Hamiltonian at the vacuum region. H_b^{GW} is bulk-like because $W_{bulk}(r,r',\omega)$ will produce a bulk Σ_b in eq 4, and the total electrostatic potential combining the nuclear and the electron charge terms in eq 4 is also bulk-like inside the nanostructure due to long-range cancellation of these two terms. As a result H_b^{GW} is equivalent to $\{-1/2\nabla^2 + V\}$ in eq 2. Next we must show that $\Sigma_P(r,r',\epsilon_i)$ in eq 8 is like the $\pm P(r)$ in eq 2. $\Sigma_P(r,r',\epsilon_i)$ is the result of eq 5 by replacing $W(r,r',\omega)$ with $P_M(r,r',\omega)$. First, we make a static approximation of $P_M(r,r',\omega) = P_M(r,r')$, dropping its ω dependence. Note that by the definition of eq 3, $P_M(r,r) = 2P(r)$. Let us first look at the first term of $\Sigma_P(r,r',\epsilon_i)$ in eq 5 (which is called the screened exchange term Σ_P^{SEX}). If we apply an quasiparticle eigen wave function ψ_i onto Σ_P^{SEX}, we have

$$\int \Sigma_P^{SEX}(r,r')\psi_i(r')\,d^3r' = -\int \sum_j \psi_j(r)\psi_j^*(r')f_j P_M(r,r')\psi_i(r')\,d^3r' \tag{9}$$

Inside the nanostructure, like other intensity functions summing over the occupied states (e.g., the charge density), we can assume that $\sum_j \psi_j(r)\psi_j^*(r')f_j$ is similar to its corresponding bulk density matrix $g(r,r') = \int_{BZ}\sum_n^{occ}[u_{nk}(r)e^{ikr}][u_{nk}(r')e^{ikr'}]\,d^3k$, here $u_{nk}(r)e^{ikr}$ is the bulk Bloch states of band n and k-point k, and the integral d^3k is over the first Brillouin zone. It has been proven by Kohn[15] that $\rho(r,r')$ is an exponential decay function of $r - r'$ for the 1D system with a band gap. Later, Des Cloizeaux[16] also proved that $\rho(r,r')$ decays exponentially for a general 3D system with a band gap. In the short range, $\rho(r,r')$ decays significantly beyond a bond length. This is shown in Figure 1 for the CdSe system we are going to study. Thus, overall, $\sum_j \psi_j(r)\psi_j^*(r')f_j$ is a short-range function of $r - r'$. However, within this short range, $P_M(r,r')$ can be replaced by $P_M(r,r)$ since (unlike W_{bulk}) $P_M(r,r')$ is a slowly varying smooth function of $r - r'$ for small $|r - r'|$. If we substitute this into eq 9, and use $\int \psi_j^*(r')\psi_i(r')\,d^3r' = \delta_{i,j}$, we have

$$\int \Sigma_P^{SEX}(r,r')\psi_i(r')\,d^3r' = -2f_i P(r)\psi_i(r) \tag{10}$$

The second term in eq 5 is often called the Coulomb hole term (COH) Σ^{COH}. It is well-known that,[17] under the static Coulomb hole approximation, it can be written as

$$\Sigma^{COH}(r,r') = \delta(r - r')\frac{1}{2}[W(r,r',0) - v(r,r')] \tag{11}$$

here $v(r,r') = 1/|r - r'|$ is the Coulomb potential. Thus the Σ_P^{COH} caused by P_M is just $\Sigma^{COH} - \Sigma_{bulk}^{COH} = \delta(r - r')P(r)$. As a result, adding it to eq 10, we have

$$\int \Sigma_P(r,r')\psi_i(r')\,d^3r' = (1 - 2f_i)P(r)\psi_i(r) \tag{12}$$

Since f_i equals 1 for valence states, and 0 for conduction band states, this is the same term as the $\pm P(r)$ in eq 2. The above derivation is based on several approximations, most noticeably the static approximation in $W(r,r',\omega)$ and the approximation from eq 9 to eq 10 by replacing $P_M(r,r')$ with $P_M(r,r)$ due to the short range of $\sum_j \psi_j(r)\psi_j^*(r')f_j$. While some approximations (e.g., the static approximation in the bulk) have been well studied, some others are not, especially in the context of a nanostructure. It will be the topic of future research to investigate the accuracies of these approximations. Here, we have just pointed out the connection between eq 2, which was originally derived classically,[11] and the many-body GW eq 4.

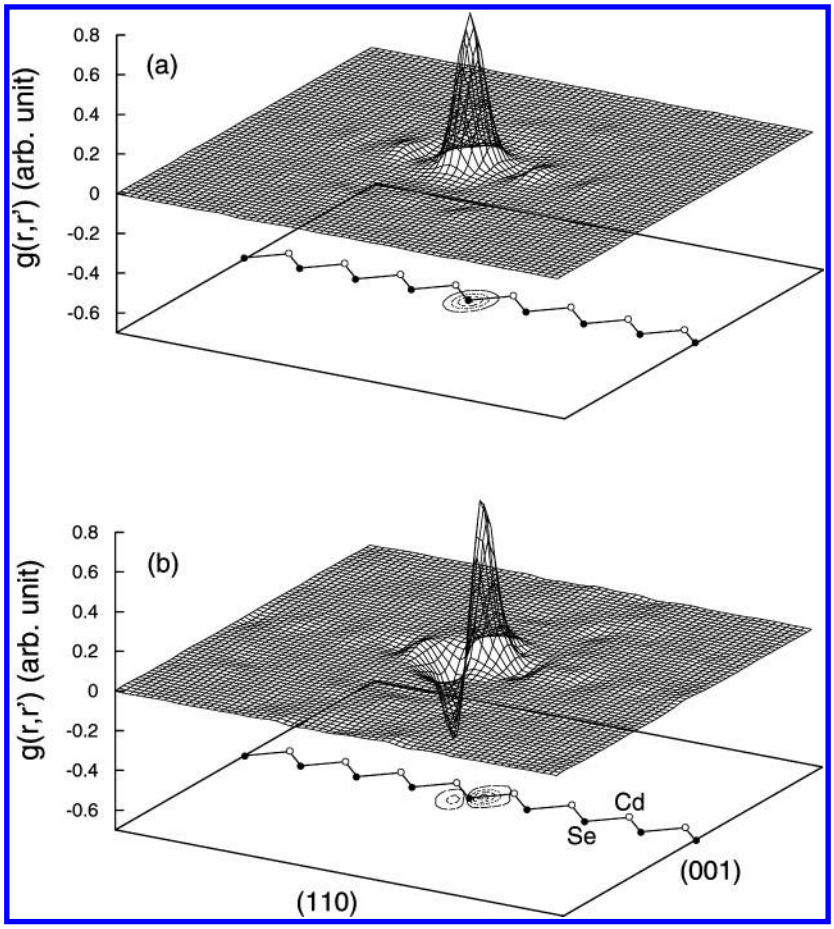

Figure 1. The $g(r,r')$ (defined in the text) of a bulk CdSe calculated by using the SEPM Hamiltonian. The $g(r,r')$ on the (110) plane cross section of a 512 atom supercell is shown. (a) $g(r,r')$ for r' located on top of a Se atom; (b) $g(r,r')$ for r' at the center of a Cd−Se bond. Only one Cd−Se bond chain is shown for clarity. The contour levels at the bottom of the graph are 0.1, 0.3, 0.5, 0.7 for part a and −0.3, −0.1, 0.1, 0.3, 0.5, 0.7 for part b.

We now will use eq 2 to solve the quasiparticle wave functions and energies. To generate $P(r)$, we first need to solve $W(r',r)$. For this purpose, we will first solve the electrostatic potential $\phi(r)$ caused by a charge density $\rho(r)$ under an inhomogeneous dielectric medium $\epsilon(r)$

$$\nabla\cdot[\epsilon(r)\nabla\phi(r)] = 4\pi\rho(r) \tag{13}$$

In this work, we will ignore the $r - r'$ dependence of $\epsilon(r)$ as in eq 6. What we are interested in here is the Coulomb interaction, not the exchange interaction between the electron and hole states, thus the short-range screening behavior is not important here.[18] Equation 13 is solved iteratively as

$$\nabla^2\phi(r) = \{4\pi\rho(r) - \nabla\epsilon(r)\cdot\nabla\phi(r)\}/\epsilon(r) \tag{14}$$

treating the whole right-hand side as a charge density. The ∇ and the inversion of ∇^2 are carried out with Fast Fourier Transform and a special technique that cuts off the range of Coulomb interaction to avoid the periodic image effects. Typically 12−15 iterations of eq 14 are enough to converge $\phi(r)$ to 10^{-4} voltage.

Following our recent study of the dielectric response in a nanostructure,[19] we have adopted a model dielectric function $\epsilon(r)$ for our tetrapod. It has a constant value of bulk dielectric constant ϵ_b (taken as 10 for CdSe in our calculation) inside the tetrapod, a 2.86 Å thick smooth transition region near the surface, and a value of 1 outside the tetrapod. An isosurface plot of $\epsilon(r)$ together with the CdSe atoms are shown in Figure 2. The tetrapod, which contains 2817 atoms, has arms 2.2 nm in diameter and 4.6 nm in length. To obtain $W(r',r)$ of eq 3, we have placed a sharp (0.86 Å width) Gaussian charge distribution at r and solved $\phi(r') = W(r',r)$ of eq 13. We have calculated $P(r)$ at 108 different r points along the arm axis and central sphere and arm radial directions, and fit the results to two separate analytical expressions in the arm and central sphere regions. The average error of the fit is about 20 meV inside the tetrapod. An isosurface and a cross section plot of the fitted $P(r)$ is shown in Figure 3. The sharp radial edges in the plot outside the tetrapod are due to the mismatch of the two analytical

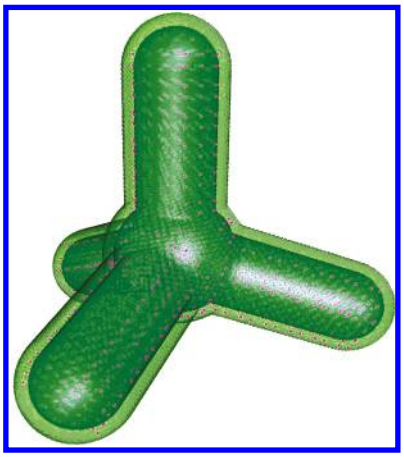

Figure 2. The model $\epsilon(r)$ of the tetrapod. The inner isosurface is for $\epsilon(r) = 0.99\epsilon_b$, where ϵ_b is the bulk dielectric constant of CdSe, and the outside isosurface is for $\epsilon(r) = 1.1$. The small pink dots are the atoms.

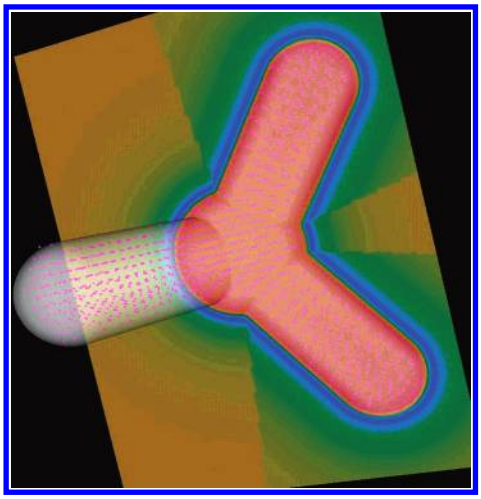

Figure 3. An isosurface and a cross section plot of the fitted polarization potential $P(r)$. The gray isosurface is for $P(r) = 0$. On the cross section, blue and green colors mean negative, while the pink color means positive. The sharp edges outside the tetrapod are due to mismatch of the fitted formula from different regions.

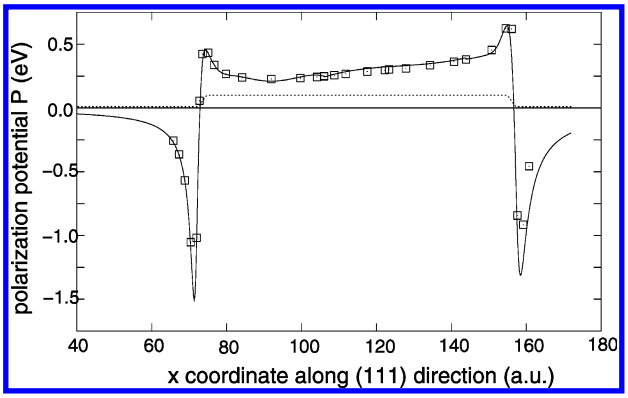

Figure 4. The polarization potential $P(r)$ along the central axis of one arm of the tetrapod. The axis line is along (x,x,x), where x is plotted as the horizontal axis. The solid line is the fitted result, while the square symbols are the results calculated directly by using eq 3. The dotted line indicates $\epsilon(r)$ (in arbitrary unit) along the axis. The center of the central sphere is at $x = 92$ au, and the arm is from $x \sim 105$ to 155 au.

expressions in that region. A line plot of $P(r)$ along the central axis of one arm is shown in Figure 4. There is a sharp positive/negative jump near the surface, typical for an image potential, and $P(r)$ is significantly smaller near the center of the sphere as compared to the arm regions.

Next, we used the fitted $P(r)$ in eq 2 to solve the quasiparticle eigen wave functions and eigen energies. The first few conduction band wave functions are shown in Figure 5, and the valence band wave functions are shown in Figure 6. In Figure 5 and 6, the quasiparticle wave functions of eq 2 are compared with the wave functions solved from eq 1 without $P(r)$. We see that there are some significant changes in the wave functions. Primarily, the wave functions are compressed toward the center of the tetrapod, due to the smaller value of $P(r)$ at the center, as mentioned above. In some cases, the addition of $P(r)$ changes the order of the states. For example, as shown in Figure 6, without $P(r)$ the VB3 (the third valence state) state has a higher energy than the degerated VB4 and VB5 states. However, after $P(r)$ is added, the original VB4 and VB5 states become the new (lower panel in Figure 6) VB3 and VB4 states, while the original VB3 state becomes the new VB5 state.

The quasiparticle eigen energies of eq 2 are shown in Figure 7, in comparison with the original single particle eigen energies of eq 1. One can see from Figure 7 that the band gap increased

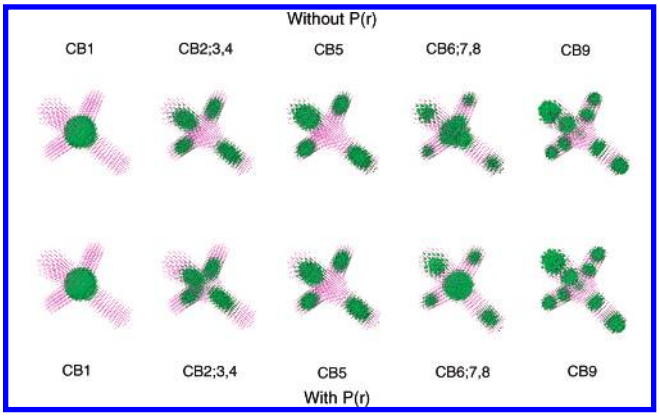

Figure 5. The isosurface plots of wave function squares of conduction band (CB) eigen states without $P(r)$ (upper panels) and with $P(r)$ (lower panels). CB3 and CB4 are degenerated (they are denoted as CB3,4), so are CB7 and CB8. CB2 and (CB3+CB4)/2 are almost indistinguishable, thus they are shown in one plot. The same is true for CB6 and (CB7+CB8)/2. The isosurface value is 0.0003 electron/Bohr^3 for all the plots. The small pink dots denote the atoms.

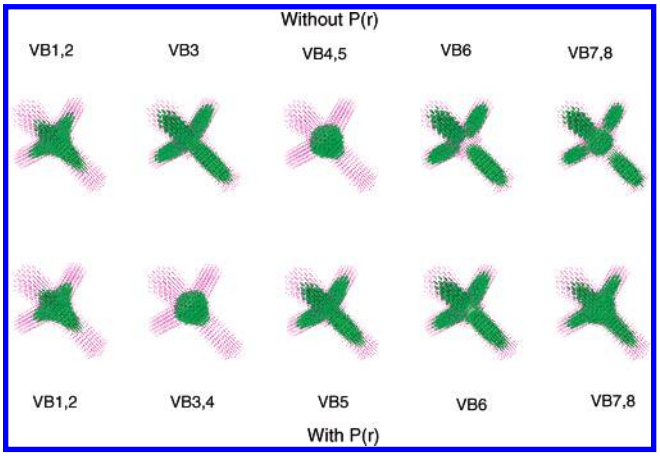

Figure 6. The isosurface plots of wave function squares of valence band (VB) eigen states, same as in Figure 5. VB1,2 means VB1 and VB2 are degenerated and the isosurface is for (VB1+VB2)/2. The same notation applies to VB4,5; VB7,8; and VB3,4. The isosurface value is 0.0003 electron/Bohr^3 for all the plots. The small pink dots denote the atoms.

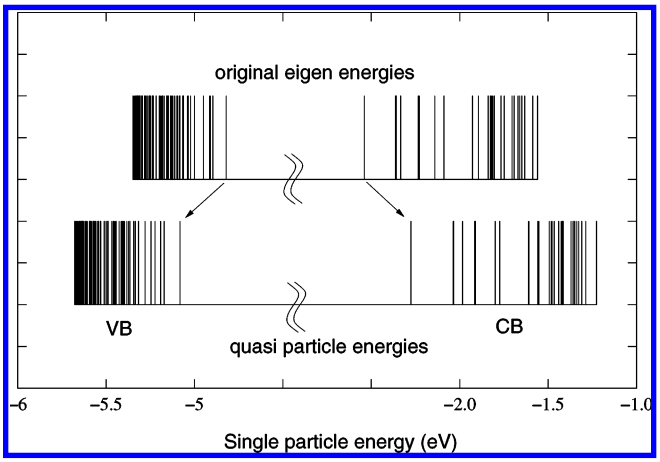

Figure 7. The eigen energies with $P(r)$ (lower bars) and without $P(r)$ (upper bars).

by about 0.5 eV from the original band gap when $P(r)$ is not used, to the new quasiparticle band gap when $P(r)$ is used. Eighty valence band states and forty conduction band states are calculated (without counting the spin Kramer doubling degeneracy). After the electron−hole Coulomb interactions $J_{i,j} =$

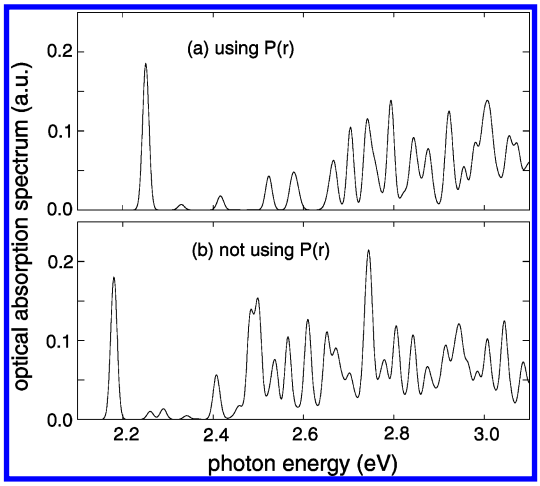

Figure 8. The optical absorption spectrum of the tetrapod with use of the current approach of $P(r)$ (a) and the approach without $P(r)$ (b). All the x,y,z polarizations are included in the optical oscillator strength.

$\int|\psi_i^{cb}(r)|^2\phi_j(r)\ d^3r$ (where $\phi_j(r)$ is the electrostatic potential caused by $\rho(r) = |\psi_j^{vb}(r)|^2$ in eq 13) is added to the exciton energy, the optical absorption spectrum can be calculated as

$$I(E) = \sum_{i,j}|\langle\psi_i^{cb}|\nabla|\psi_j^{vb}\rangle|^2\delta(\epsilon_i^{cb} - \epsilon_j^{vb} - J_{i,j} - E), \quad (15)$$

here $|\langle\psi_i^{cb}|\nabla|\psi_j^{vb}\rangle|^2$ is the optical oscillator strength. This can be considered as the zeroth order application of the Bethe−Salpeter equation.[20] When the exciton correlation effects are not strong comparing to the single particle confinement (strong confinement case), as in our current system, the zeroth order approximation is fairly accurate.[21] The resulting $I(E)$ with 10 meV broadening for the δ function is shown in Figure 8a. In Figure 8b we show a similar result calculated with wave functions ψ_i and eigen energies E_i of eq 1, and the Coulomb interaction $J_{i,j}^{bulk}$ is calculated with a uniform $\epsilon(r)$ equal to the bulk dielectric constant ϵ_b. This is the procedure typically used for simple convex nanosystems (e.g., spherical quantum dots), based on the justification that the single particle energy changes caused by the $\pm P(r)$ term in eq 2 will cancel the extra electron−hole Coulomb interaction caused by the P_M term in eq 7.[4,11,22] However, for the nonconvex tetrapod studied here, we find that this is not true, and the residual of this cancellation is as large as the $J_{i,j}^{bulk}$ itself. For example, for the CB1 and VB1 states, the quasiparticle $\epsilon_{CBM} - \epsilon_{VBM} - J_{C,V}$ is 2.251 eV, while the original formula $E_{CBM} - E_{VBM} - J_{C,V}^{bulk}$ has a value of 2.180 eV. Their difference of 0.07 eV is almost as large as the $J_{C,V}^{bulk} = 0.1$ eV. We also see that the absorption spectra calculated by using these two approaches are quite different [Figure 8a,b], especially for the higher energy peaks. Thus, in our case, it is important to solve eq 2, instead of eq 1. We suspect this will be true for most complex nonconvex nanosystems.

Finally, we use the current approach to calculate the electron and hole addition energies. The addition energy Δ_N is defined as the change of the Fermi energy μ_{N+1} from μ_N, while μ_N is the energy needed to add one more electron (or hole) into a $N - 1$ electron (hole) system. Here for the neutral system, $N = 0$. By definition $\mu_N = E_{tot}(N) - E_{tot}(N-1)$ and $E_{tot}(N)$ is the total energy of a N additional electron (or hole) nanosystem. Thus, we have

$$\Delta_N = E_{tot}(N+1) + E_{tot}(N-1) - 2E_{tot}(N) \quad (16)$$

In the zeroth order approximation, $E_{tot}(N)$ equals the sum of the single particle eigen energies $\sum^i\epsilon_i$ plus the electron−electron (or hole−hole) Coulomb interactions. In a more general expression, a Coulomb interaction can be expressed between four single particle wave functions as $J_{i,i',j,j'} = \int\psi_i(r)\psi_{i'}^*(r)\phi_{jj'}(r)\ d^3r$, and $\phi_{jj'}(r)$ is the solution of eq 13 with $\rho(r) = \psi_j^*(r)\psi_{j'}(r)$. After all the possible $J_{i,i',j,j'}$ values have been calculated, the Coulomb interaction between any two different N-electron Slater determinants (configurations) can be calculated, thus a configuration interaction (CI) diagonalization is possible among all the N-electron Slater determinants. The details of this approach can be found in ref 23. We have used this procedure to calculate the total energies $E_{tot}(N)$ up to $N = 24$. However, in the CI calculation, due to the large computational requirement, it is impossible to include all the possible Slater determinants. As a result, to calculate Δ_N for $N = 1, 2$, we have included all the possible configurations constructed from the first 12 single particle states (24 counting the spin); for $N = 3, 4, 5$, all the configurations from the first 8 states; for $N = 6$ to 12, all the configurations from the first 7 states; and for $N > 7$, only a single Slater determinant. For a given Δ_N, the three E_{tot} for $N + 1$, N, and $N - 1$ in eq 16 have been calculated by using the same scheme (e.g., using all the Slater determinants from the 12 single particle states) for possible error cancellations. Nevertheless, we find that the Δ_N calculated in this approach is not completely converged for large N with regard to the number of configurations used. Using different configuration schemes, the resulting Δ_N can differ by more than 0.1 eV. In the future, other approaches may be explored to calculate $E_{tot}(N)$, for example, to calculate the extra N electron self-consistently according to density functional theory.[5] This situation is different from the single exciton case in the absorption spectrum of Figure 8, since the wave function relaxation and correlation effects are large, due to the large numbers of electrons (or holes).

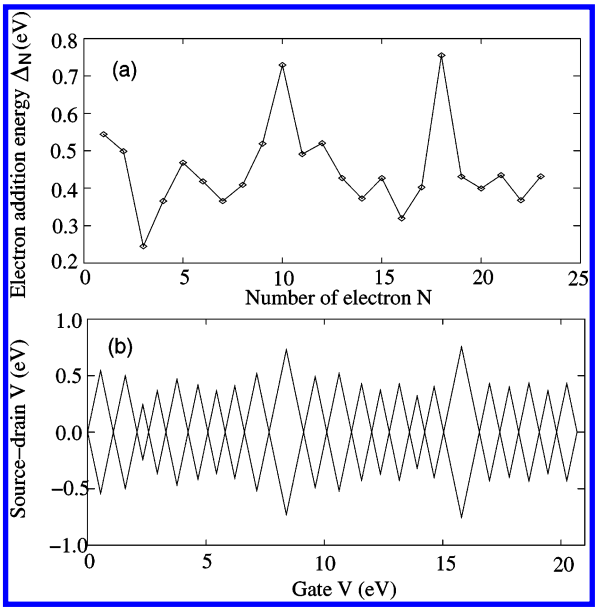

Figure 9. The addition energies of electrons (a) and the corresponding Coulomb blockade diamond structures (b). To construct the diamond structure of a given N, we have taken the Δ_N as the height of the diamond and $2\Delta_N$ as the base width of the diamond.

Despite of the possible inconvergence for large N, we have plotted Δ_N for electrons and holes in Figure 9a and Figure 10a, respectively, for N up to 24. The Δ_N for the first few N are more reliable because large numbers of configurations are used. We see that the Δ_N is not a constant. Unlike the change of Δ_N in an spherical quantum dot, which is mostly caused by the discrete single particle energy levels,[2] here the change of Δ_N is

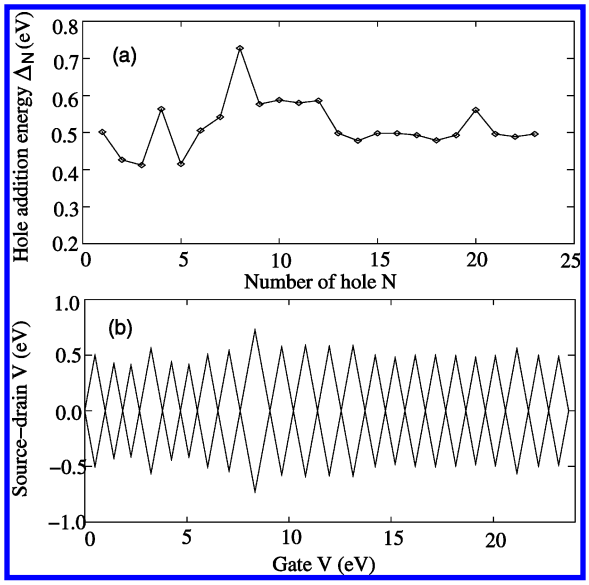

Figure 10. The addition energies of holes (a) and the corresponding Coulomb blockade diamond structures (b), same as in Figure 9.

mainly due to the different electron−electron Coulomb interactions between different states. For example, as can be seen from Figure 7, the second electron state is higher than the first electron state by about 0.25 eV. If the electron−electron Coulomb energy were the same between all the states, then Δ_2 (which corresponds to adding the third electron) should be higher than Δ_1 by this amount. This is exactly what occurs in a spherical quantum dot.[2] But in our case, Δ_2 is slightly lower than Δ_1, as can be seen in Figure 9a. This is because, as shown in Figure 5, the second electron state is outside in the arms, while the first state is at the center. As a result, the Coulomb interaction between the second and the first state is small, which reduces Δ_2. For Δ_3 (which corresponds to adding the fourth electron into the system), due to the near degeneracy of CB2, CB3, and CB4, it becomes possible to arrange one electron at one arm, and another electron at another arm. As a result, the interaction between the third and the fourth electron is very small, causing a large drop in Δ_3. Another distinct feature of the electron Δ_N is the two peaks at $N = 10$ and 18. The $N = 10$ peak is likely related to the spatial location of the CB6 state (which is needed when the 11th electron is added). As shown in Figure 5, CB6 has a large density at the center, resulting in a large Coulomb interaction with the occupied CB1 state. Comparing the electron Δ_N in Figure 9a with the hole Δ_N in Figure 10a, we found that the variation of the electron addition energies is much larger than that of the hole addition energies.

The addition energy is often related to Coulomb blockade in electron transport.[1] The Coulomb blockade diamond structures corresponding to our calculated addition energies are plotted in Figures 9b and 10b for electron and hole, respectively. For a single dot transport setup, the areas inside one diamond cannot conduct current, and thus it is Coulomb blockaded. We see that in our tetrapod case, especially for electrons, there are different sizes of diamonds. For large and convex quantum dots, the sizes of the diamonds (the values of the addition energies) are essentially uniform. Recently, the transport current and the Coulomb blockade curves for CdTe tetrapods were experimentally measured.[10] Two possible behaviors were observed for a tetrapod: one is a weakly coupled multiple dots behavior, and another is a coherently coupled single dot carrier delocalization behavior. In the weakly coupled multiple dots case, it is proposed that the carrier hops from one part of the tetrapod (e.g., the arm) to another part (e.g., the central sphere). The calculations presented here correspond to the coherently coupled single dot scenario. Similar to the experimental observations, we find variations in the addition energies for different N. However, we have to keep in mind the big difference of the sizes between the calculated tetrapod (2.2 nm in diameter and 4.6 nm in arm length) and the experimental tetrapod (8 nm in diameter and 150 nm in arm length). To accurately simulate the experiment, one also needs to include the effects of the metal electrode and surrounding medium, especially for their effects on $P(r)$.

In conclusion, we have shown that the quasiparticle eq 2, previously derived by using classical electrostatic arguments, can be derived from the GW many-body equations under appropriate approximations. We also show that for nonconvex nanosystems, such as tetrapods, eq 2 instead of eq 1 should be used even for optical gap and absorption spectrum calculations. The polarization potential $P(r)$ can significantly change the electron wave functions. Finally, we find that, in contrast with a spherical quantum dot, the addition energy of a tetrapod is not a constant, and the sizes of the Coulomb blockade diamond structures are not uniform. This variation of the addition energy is mainly caused by the different spatial locations of the quasiparticle states, not by the discrete quasiparticle energies.

Acknowledgment. The author thanks Dr. J. Li for providing the initial wave functions from previous SEPM calculations, and Dr. A. Franceschetti for use of the CI diagonalization program. This work was supported by U.S. Department of Energy, OER-BES, under Contract No. DE-AC03-76SF00098. This research used the resources of the National Energy Research Scientific Computing Center.

References and Notes

(1) Grabert, H.; Devoret, M. H. *Single charge Tunneling*: *Coulomb blockade Phenomena in Nanostructures*; Plenum Press: New York, 1992.
(2) Franceschetti, A.; Zunger, A. *Phys. Rev. B* **200**, *62*, 2614.
(3) Franceschetti, A.; Zunger, A. *Phys. Rev. Lett.* **1997**, *78*, 915.
(4) Fonaberov, V. A.; Pokatilov, E. P.; Balandin, A. A. *Phys. Rev. B* **2002**, *66*, 85310.
(5) Stopa, M. *Phys. Rev. B* **1996**, *54*, 13767.
(6) Manna, L.; Scher, E. C.; Alivisatos, A. P. *J. Am. Chem. Soc.* **2000**, *122*, 12700.
(7) Manna, L.; Milliron, D. J.; Meisel, A.; Scher, E. C.; Alivisatos, A. P. *Nat. Mater.* **2003**, *2*, 382.
(8) Huynh, W. U.; Dittmer, J. J.; Alivisatos, A. P. *Science* **2002**, *295*, 2425.
(9) Sun, B.; Marx, E.; Greenham, N. C. *Nano Lett.* **2003**, *3*, 961.
(10) Cui, Y.; Banin, U.; Bjork, M. T.; Alivisatos, A. P. *Nano Lett.* **2005**, *5*, 1519.
(11) Brus, L. E. *J. Chem. Phys.* **1983**, *79*, 5566. Brus, L. E. *J. Chem. Phys.* **1986**, *80*, 4403. Brus, L. E. *J. Chem. Phys.* **1986**, *90*, 2444.
(12) Li, J.; Wang, L. W. *Nano Lett.* **2003**, *3*, 1357.
(13) Wang, L. W.; Zunger, A. *Phys. Rev. B* **1996**, *53*, 9579.
(14) Hedin, L.; Lundqvist, S. In *Solid State Physics*, *Advances in Research and Application*; Seitz, F., Turnbull, D., Ehrenreich, H., Eds.; Academic Press: New York, 1969; Vol. 23, p 1.
(15) Kohn, W. *Phys. Rev.* **1959**, *115*, 809.
(16) Des Cloizeaux, J. *Phys. Rev.* **1964**, *135*, A685.
(17) Hybertsen, M. S.; Louie, S. G. *Phys. Rev. B* **1984**, *34*, 5390.
(18) Franceschetti, A.; Wang, L. W.; Fu, H.; Zunger, A. *Phys. Rev. B* **1998**, *58*, R13367.
(19) Cartoixa, X.; Wang, L. W. *Phys. Rev. Lett.* **2005**, *94*, 236804.
(20) Strinati, G. *Phys. Rev. B* **1984**, *29*, 5718.
(21) Shumway, J.; Franceschetti, A.; Zunger, A. *Phys. Rev. B* **2001**, *63*, 155316.
(22) Delerue, C.; Allan, G.; Lannoo, M. *Phys. Rev. Lett.* **2003**, *90*, 76803.
(23) Franceschetti, A.; Fu, H.; Wang, L. W.; Zunger, A. *Phys. Rev. B* **1999**, *60*, 1819.